RSC Advances

PAPER

View Article Online
View Journal | View Issue

Cite this: *RSC Adv.*, 2017, **7**, 51822

Size-controlled synthesis of Cu_2O nanoparticles: size effect on antibacterial activity and application as a photocatalyst for highly efficient H_2O_2 evolution†

Liangbin Xiong,*[a] Huaqing Yu,*[a] Changjiang Nie,[a] Yongjun Xiao,[a] Qingdong Zeng,[a] Guangjin Wang,[c] Boyun Wang,[a] Hao Lv,[a] Qianguang Li[a] and Shunsheng Chen*[b]

We propose a green approach for the size-controlled synthesis of Cu_2O nanoparticles (NPs) with simplified chemical deposition technology by adjusting the concentration of the precursor copper source. The morphologies, phase compositions and structures were recorded for the obtained Cu_2O NPs with sizes of 10, 50, 100 and 200 nm. In the dark, all of the Cu_2O NPs showed good antibacterial activity towards *Escherichia coli* K-12 (*E. coli*). A size-dependent antibacterial effect was also observed as a result where decreasing the size of the Cu_2O NPs led to increasing the antibacterial activity. The smallest Cu_2O NPs (Cu_2O-10) with the minimum inhibitory concentration ($\leq$1 μg mL^{-1}) achieved the highest antibacterial efficiency, with the inactivation of 7-log *E. coli* in 80 min with a concentration of 5 μg mL^{-1} in the dark. Under visible light (VL), medium concentrations (10, 20 and 50 μg mL^{-1}) of Cu_2O-10 showed enhanced antibacterial activity compared to that in the dark. For low (5 μg mL^{-1}) or high concentrations (200 μg mL^{-1}) of Cu_2O-10, the antibacterial activity under VL was almost the same as that in the dark. The mechanisms of antibacterial activity are proposed and discussed in detail. "Contact killing" and photogenerated h^+ together with reactive oxygen species (such as $^{\bullet}OH$ and H_2O_2) were found to be responsible for bacterial inactivation in the dark and under irradiation, respectively. Cu_2O-10 proved to be a good photocatalyst, capable of the highly efficient evolution of H_2O_2, whose stable equilibrium concentration could be as high as 150 μM (using 20 μg mL^{-1} of Cu_2O-10). Study on the membrane-separated system shows that the concentration of diffusing H_2O_2 can be as high as 50 μM, contributing to a complete inactivation of 7-log *E. coli* in 7 h. For comparison, the inactivation kinetics of the Cu_2O NPs and H_2O_2 were calculated, and could be fitted into the Weibull and shoulder-linear-tail models, respectively.

Received 25th September 2017
Accepted 23rd October 2017

DOI: 10.1039/c7ra10605j

rsc.li/rsc-advances

1. Introduction

Synthesis of cuprous oxide (Cu_2O) nanostructures is becoming increasingly attractive due to their relatively easy preparation, low cost and wide range of potential applications. In particular, shape-controlled synthesis of Cu_2O nanostructures has been extensively studied because precise control of shapes offers an opportunity for discovering potentially exciting and unique shape-dependent properties.[1] As a result, a wide variety of Cu_2O nanostructures with controlled shapes such as rods,[2] wires,[3] spheres,[4] different polyhedrals[5–8] and hollow structures[9–11] have been successfully synthesized, and some shape-dependent properties have been widely investigated as well.[12–14] However, a size-controlled synthesis of Cu_2O nanoparticles (NPs) has so far been absent and remains a challenging task owing to the intrinsic difficulties in controlling the sizes of NPs while keeping their shapes uniform and unchanged. Thus, the size-controlled synthesis of Cu_2O NPs is highly interesting not only for further development of synthetic strategies, but also for the examination of their size-dependent properties.

Cu_2O NPs, which are a good antibacterial, are widely used as an antiseptic and germicide in daily life[15] and are a promising antibacterial for medical treatment[16] and the removal of pathogens from aquatic environments.[17] In recent years, the

[a]*School of Physics and Electronic-Information Engineering, Hubei Engineering University, Xiaogan, 432000, China. E-mail: Xiong_lb@yahoo.com; yuhuaqing@126.com*

[b]*Institute for Quantum Materials, School of Mathematics and Physics, Hubei Polytechnic University, Huangshi, 435003, China. E-mail: chenshunsheng75@163.com*

[c]*College of Chemistry and Materials Science, Hubei Engineering University, Xiaogan, 432000, China*

† Electronic supplementary information (ESI) available. See DOI: 10.1039/c7ra10605j

engineering of micro- and nanostructures of Cu_2O has tended to attract particular interest owing to their distinctive and outstanding antibacterial activity. Microstructured Cu_2O was found to have morphology-dependent antibacterial activity and specificity against Gram-positive and Gram-negative bacterial strains.[17–20] Nanostructured Cu_2O was studied and demonstrated higher antibacterial activity than its high valence counterpart (CuO)[21,22] and even most metal oxide NPs such as TiO_2,[21] ZnO,[21,23] WO_3[21] and NiO.[23] However, there has still been a lack of studies on the relationship between the antibacterial activity and particle size of Cu_2O NPs. Thus, in this study, we initiate an investigation on the effect of size on the antibacterial activity of Cu_2O NPs towards *Escherichia coli* K-12 (*E. coli*) in the dark.

Cu_2O NPs are also an efficient visible-light-driven photocatalyst with a high absorption coefficient and theoretical solar conversion efficiency. However, studies on pristine Cu_2O NPs only center on either the photocatalytic degradation of organics[10,24,25] or H_2 production,[26–28] and their application in photocatalytic water disinfection has not been reported till now. Moreover, the excellent photocatalytic degradation activity of organics suggests that Cu_2O NPs might have high photoactive antibacterial effects, inspiring us to further investigate their properties and functions related to photoactive antibacterial effects under visible light (VL).

In this study, we developed an effective protocol for the size-controlled preparation of Cu_2O NPs by improving a previous chemical deposition method[29] at ambient temperature without a high energy demand, complicated apparatus, or any organic compounds or surfactants. In particular, we paid much attention to the inactivation kinetics of H_2O_2 towards *E. coli* because H_2O_2 is widely involved in Cu_2O[29–31] and Cu_2O-based[32] photocatalytic systems but its role is still unclear for photocatalytic disinfection. Moreover, for comparison, the rates of inactivation of *E. coli* in different conditions were calculated and fitted according to the inactivation kinetics of models proposed by Geeraerd *et al.* (2000).[33] We expect that this study can offer a significant reference for the selection of Cu_2O in real applications.

2. Experimental section

2.1. Preparation and characterization of Cu_2O NPs

A stock colorless 500 mL solution was prepared by adding 400 mL of sodium thiosulfate ($Na_2S_2O_3$) to 100 mL of copper sulfate ($CuSO_4 \cdot 5H_2O$) solution. The concentrations of $CuSO_4 \cdot 5H_2O$ were adjusted to 0.05, 0.1, 0.6, 1, 1.2 and 2 M. The concentrations of $Na_2S_2O_3$ were adjusted correspondingly and the molar ratio of $CuSO_4 \cdot 5H_2O$ and $Na_2S_2O_3$ was fixed at 1 : 4. The same volume (500 mL) of 5 M NaOH solution was placed in another beaker. The mixture was poured into the above NaOH solution with vigorous stirring. Cu_2O powder was obtained by centrifugation at 12 000 rpm, washed with deionized water and dried under vacuum at 60 °C. The phase purity of the Cu_2O powder was characterized by X-ray powder diffraction (XRD) using an X-ray diffractometer (Y-2000) with Cu Kα radiation ($\lambda = 1.5418$ Å). A scan efficiency of 0.1° S^{-1} was applied to record the powder patterns in the range of $10° \leq 2\theta \leq 80°$. The Brunauer–Emmett–Teller (BET) surface areas of the samples were determined by a high-speed automated area and pore size analyzer (NOVA 2000e). Scanning electron microscopy (SEM) images were obtained on a JEOL SM-6700F microscope operating at 5 kV. Transmission electron microscopy (TEM) and high-resolution transmission electron microscopy (HRTEM) were carried out with a JEOL JEM-100CXII.

2.2. Bacterial inactivation by Cu_2O NPs in the dark and under VL irradiation

The inactivation of *E. coli* was conducted using a 300 W xenon lamp (Beijing Perfect Light Co. Ltd., Beijing) with a UV cutoff filter ($\lambda < 400$ nm) as the light source (Fig. S1†). The VL intensity was measured by a light meter (LI-COR, USA) and adjusted to 100 mW cm^{-2}. The bacteria strain *E. coli* was received from the American Type Culture Collection and chosen for this study. One pure bacterial colony grown on the nutrient agar plate was inoculated in a 2.5% nutrient broth solution at 37 °C with 200 rpm agitation for 17 h. The culture was then washed twice with sterilized 0.9% NaCl solution (saline) by centrifugation at 5000 rpm for 5 min using a Hermle Z323 centrifuge (Hermle Labortechnik, Germany). The bacterial cells and Cu_2O NPs were suspended in saline in a partly-filled beaker and the cell density was finally adjusted to about 2×10^7 colony forming unit (cfu) per mL or 2×10^5 cfu mL^{-1} by dilution with an appropriate volume of saline to conduct different antibacterial experiments. The reaction temperature was maintained at 25 °C. At different time intervals, aliquots of the sample were collected and serially diluted with saline. 0.1 mL of the diluted sample was then immediately spread on nutrient agar (Lancashire, UK) plates and incubated at 37 °C for 24 h to determine the number of viable cells (in cfu). Light controls (light alone without Cu_2O NPs) and dark controls (without Cu_2O NPs and light) were also carried out for each set of experiments. All of the experimental controls and treatments were performed in triplicates.

To compare the rate of inactivation of *E. coli*, the inactivation kinetics in different conditions were calculated using the GInaFit software according to the microbial survival models proposed by Geeraerd *et al.*[33] Two models were used in this study named the Weibull and shoulder-linear, which can be referred to as eqn (1) and (2), respectively.

$$\log 10(N) = \log 10(N_0) - \left(\frac{t}{\delta}\right)^p \quad (1)$$

where N_0 and N are the initial and surviving number of cells (log, in cfu), respectively, t = reaction time [min] and δ [time unit] is a scale parameter.

$$\log(N) = \log\left[\left(10^{\log(N_0)} - 10^{\log(N_{res})}\right) \times e^{-K_{max}t} \times \frac{e^{(K_{max}S_l)}}{1 + (e^{K_{max}S_l} - 1) \times e^{(-K_{max}t)}} + 10^{\log(N_{res})}\right] \quad (2)$$

where K_{max} = specific inactivation rate [min^{-1}], S_l = shoulder length [min], N_{res} = residue population density [cfu mL^{-1}], N_0

and N are the initial and surviving number of cells (log, in cfu), respectively, and t = reaction time [min].

2.3. Fluorescence spectroscopy

The membrane-separated (or partition) system is shown in Fig. S2.† The *E. coli* in no-Cu_2O cell with different irradiation times was collected and stained with the dyes of the LIVE/DEAD BacLight bacterial viability kit (L7012, Molecular Probes, Inc. Eugene, OR) following the protocol recommended by the manufacture. After being incubated at 25 °C for 15 min in the dark, the samples were transferred to a coverslip and examined with a fluorescence microscope (Nikon ECLIPSE 80i, Japan) equipped with an NUV-2A filter block consisting of an Ex 400–600 (Nikon, Japan) excitation filter and a Spot-K slider CCD camera (Diagnostic instruments. Inc. Sterling Heights, MI).

2.4. Determination of the concentrations of copper ion

The concentration of cuprous ion (Cu^+) was measured by colorimetric analysis with bathocuproine disulfonic acid, which selectively chelates Cu^+. The total concentration of the copper ion was also measured by adding ascorbic acid to reduce all of the cupric ions (Cu^{2+}) to Cu^+.[34] The corresponding absorbance spectra (457 nm) were recorded using a UV/Vis spectrophotometer (Blue Star A, US).

2.5. Detection of H_2O_2, $^{\bullet}O_2^-$ and $^{\bullet}OH$

H_2O_2 was analyzed photometrically by the peroxidase-catalyzed oxidation product of *N*,*N*-diethyl-*p*-phenylenediamine,[23,24] which was measured using a UV/Vis spectrophotometer (Blue Star A, US) at 551 nm.[31] Superoxide radical ($^{\bullet}O_2^-$) was measured by 2,3-bis(2-methoxy-4-nitro-5-sulfophehyl)-2*H*-tet-razolium-5-carboxanilide (XTT),[35–37] which can be reduced by $^{\bullet}O_2^-$ to form XTT-formazan. The formazan has an absorption spectrum (measured by a UV/Vis spectrophotometer (Blue Star A, US)) with a peak at 470 nm that can be used to quantify the relative amount of $^{\bullet}O_2^-$. Terephthalic acid (TA) is a well-known probe to detect $^{\bullet}OH$ due to its high reactivity with $^{\bullet}OH$. The reaction between TA and $^{\bullet}OH$ results in the formation of 2-hydroxy-terephthalic acid[38] which can be detected using an HPLC-FLD system.[39] The steady state concentration of the $^{\bullet}OH$ can be calculated using the following eqn (3) and (4):[40]

$$^{\bullet}OH + \text{Terephthalic acid (TA)} \rightarrow \text{2-hydroxyterephthalic acid (2HTA)} \quad (3)$$

$$\frac{d[2HTa]}{dt} = 0.35 \times k_{\cdot OH,TA} \times [TA][^{\bullet}OH] \quad (4)$$

where $k = 3.3 \times 10^9\ M^{-1}\ s^{-1}$.

3. Results and discussions

3.1. Synthesis and characterization of Cu_2O NPs

Cu_2O can be produced by a chemical deposition method[29] described in eqn (5)–(7):

$$2Cu^{2+} + 4S_2O_3^{2-} = 2[CuS_2O_3]^- + [S_4O_6]^{2-} \quad (5)$$

$$[CuS_2O_3]^- \leftrightarrow Cu^+ + S_2O_3^{2-} \quad (6)$$

$$2Cu^+ + OH^- \rightarrow Cu_2O + H^+ \quad (7)$$

In a typical procedure, NaOH, $CuSO_4 \cdot 5H_2O$ and $Na_2S_2O_3$ were introduced as source materials, in which $CuSO_4 \cdot 5H_2O$ and $Na_2S_2O_3$ were used as the precursors of the Cu_2O and reducing agent, respectively. The formation of Cu_2O can be expressed as the reaction of free Cu^+ ions with OH^- ions (eqn (7)). In this work, this deposition technique was improved and an effective protocol was developed for size-controlled preparation of the Cu_2O NPs. In the improved deposition method, a relatively high concentration of NaOH (5 M) was used to suppress the agglomeration of Cu_2O NPs due to the generation of strongly electrostatic repulsion amongst the Cu_2O NPs. Different sizes of Cu_2O NPs were successfully prepared by simply adjusting the concentration of Cu(II) in eqn (5). Here, the concentrations of $CuSO_4 \cdot 5H_2O$ as the precursor of Cu_2O were adjusted ranging from 0.05 to 2 M. Fig. 1A–D show the representative SEM images of the Cu_2O NPs prepared with concentrations of 0.1, 0.6, 1 and 1.2 M, respectively. The obtained Cu_2O NPs were uniform in size and their size distributions are shown in Fig. S3.† The corresponding sizes are around 10, 50, 100 and 200 nm, and so they were named Cu_2O-10, Cu_2O-50, Cu_2O-100 and Cu_2O-200, respectively. Increasing the concentration of precursor significantly increased the size of the Cu_2O NPs (Fig. 1A–D). However, further increasing the concentration of the precursor did not contribute to an increased size of the Cu_2O NPs. This is due to excessive copper precursor counteracting the function of NaOH for suppression of the agglomeration of the Cu_2O NPs, resulting in the agglomeration of Cu_2O NPs (Fig. 1D). A much more serious agglomeration of Cu_2O NPs was observed when using 2 M of the copper precursor (Fig. S4†) due to interconnection of these Cu_2O NPs to form irregular structures. This result was expected and is similar to that of our previous report.[29] On the

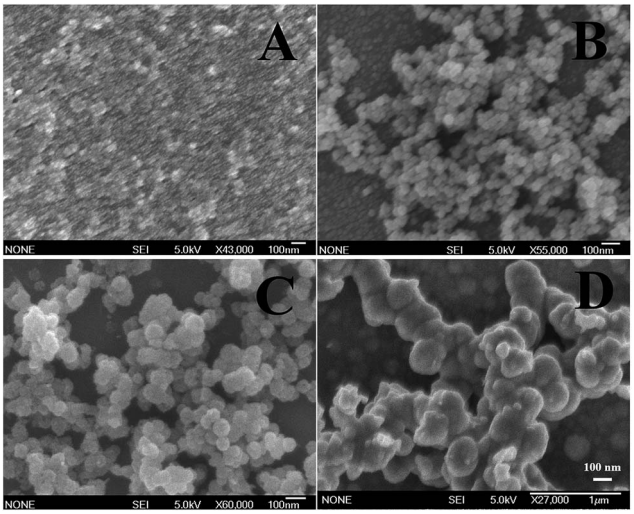

Fig. 1 SEM images of Cu_2O NPs prepared with (A) 0.1, (B) 0.6, (C) 1 and (D) 1.2 M of Cu(II) ion solution. The concentration of NaOH solution was fixed at 5 M.

other hand, an excessively low concentration of precursor failed to achieve smaller Cu_2O NPs (less than 10 nm). The SEM image of the Cu_2O NPs (not shown here) prepared with 0.05 M of precursor is similar to that with 0.1 M of precursor. The results suggest that 10 nm is close to the size of the crystal nucleus for the formation of Cu_2O NPs in the current synthesis conditions.

Fig. 2 shows the XRD pattern of Cu_2O-10. Five peaks at $2\theta =$ 29.78°, 36.56°, 42.39°, 62.51°, and 73.46° can be indexed to the (110), (111), (200), (220) and (311) planes of the Cu_2O cubic phase, which is very close to the values in the JCPDS – International Centre for Diffraction Data (PDF, Powder Diffraction File, no. 05-0667, 1996). No other peaks suggesting impurities, or significant changes in the peak locations of the XRD spectra were detected indicating that pure Cu_2O powders were obtained under the current synthetic conditions. The high intensity of the (111) diffraction peak suggests that the obtained crystals are mainly dominated by (111) facets. The XRD spectra of the other Cu_2O samples were as good as that of Cu_2O-10 (data not shown here), indicating that variation of the Cu(II) ion concentration does not change the phase composition of the Cu_2O NPs. The average size of the nanocrystals for these samples was estimated using the Debye–Scherrer formula from the full width at half maximum (FWHM) of the diffraction peaks. According to the FWHM of the diffraction peaks of the (111) plane of Cu_2O, the average size of the Cu_2O crystals was determined to be about 7.1 nm.

TEM images of Cu_2O-10, Cu_2O-50, Cu_2O-100 and Cu_2O-200 are shown in Fig. 3A–D, and display almost the same sizes as the corresponding SEM data. HRTEM was also carried out to further investigate the crystal structure of the Cu_2O NPs. Fig. 3E is a typical HRTEM image of Cu_2O-10. The Fourier transform pattern [Fig. 3E, inset (I)] corresponding to the red square region with two-dimensional lattice fringes indicates that Cu_2O-10 was composed of small single crystals with sizes of 5–10 nm. Fig. 3F shows the bright field of the HRTEM image for an individual nanosphere of Cu_2O-200. The non-uniform contrast of the HRTEM image suggests that the large nanosphere is also assembled with small crystals with sizes of about 5–10 nm (Fig. 3F inset). The results suggest that the sizes of the obtained Cu_2O NPs are different, but they are all composed of small single crystals with sizes of 5–10 nm, which is in good agreement with the size data (7.1 nm) obtained from the XRD analysis. In addition, the circle corresponding to the (111) plane is much brighter than the others in the selected area electron diffraction pattern (Fig. 3E, inset (II)), indicating that the formation of the Cu_2O NPs is highly orientated to the (111) plane and is also in agreement with the data of the XRD analysis.

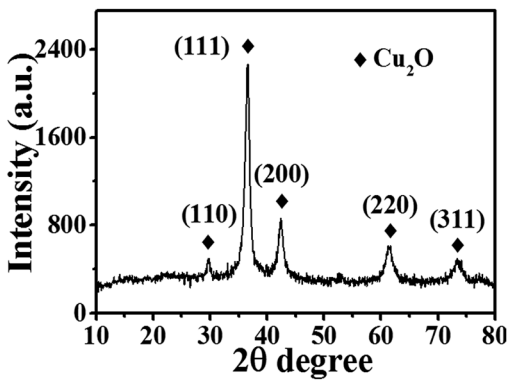

Fig. 2 XRD pattern of Cu_2O-10 NPs.

3.2. Comparison of bacterial inactivation by Cu_2O NPs with different sizes in dark

The antibacterial activity and inactivation kinetics of *E. coli* in the dark by the obtained Cu_2O NPs are shown in Fig. 4A. Control experiments confirmed that *E. coli* was not inactivated only in the dark control. A cell loss of about 2×10^7 was achieved for 20 μg mL^{-1} of Cu_2O-10, Cu_2O-50, Cu_2O-100 and Cu_2O-200 within 60, 240, 300 and 360 min, respectively, indicating that an increase in the size of the Cu_2O NPs resulted in a decrease in the antibacterial activity. They are characterized by the convex curves (dashed lines of Fig. 4A) of the Weibull model whose parameters are given in Table S1(a).† The inactivation kinetics of *E. coli* by the Cu_2O NPs in the dark are in good agreement with those of the thermal inactivation of microbial cells which can also be described by the Weibull model.[41,42] The variation of the scale parameter δ (time) indicates a negative correlation between the inactivation effects and the sizes of the Cu_2O NPs. The dimensionless parameter p denotes the shape of the fitted curves. The dashed lines of Fig. 4A are visualized as convex curves ($p > 1$, Table S1(a)†), indicating that the remaining cells became increasingly damaged.[41]

3.3. Comparison of bacterial inactivation by Cu_2O-10 with different concentrations in the dark

The antibacterial effects were further studied for different concentrations of Cu_2O-10 NPs, whose antibacterial activity and inactivation kinetics are recorded in Fig. 4B. Complete inactivation of 7-log *E. coli* by 5, 10, 20, 50, and 200 μg mL^{-1} of Cu_2O-10 was observed within 80, 70, 60, 40 and 10 min, respectively. We also determined the minimum inhibitory concentration (MIC) for Cu_2O-10 to be ≤ 1 μg mL^{-1}, which is much lower than the 6.25,[18] 100,[21] and 1270 (ref. 43) μg mL^{-1} reported for the MICs of *E. coli* in cited references. The inactivation kinetics (dashed lines of Fig. 4B) of *E. coli* were also fitted with the Weibull model (Table S1(b)†). The scale parameters $p > 1$ and δ decreased with an increase in the Cu_2O content (Table S1(b)†) indicating that the remaining cells became increasingly damaged[41] and that a high Cu_2O content resulted in a high inactivation efficiency.

3.4. Photocatalytic inactivation activity

Fig. 5 shows the photocatalytic inactivation of *E. coli* by Cu_2O-10 with different concentrations. Control experiments indicated that *E. coli* was not inactivated only under the light control. Under VL the antibacterial activity of Cu_2O-10 with a medium concentration (10, 20 and 50 μg mL^{-1}) was substantially improved, indicating that Cu_2O-10 can be driven by VL and enjoys photocatalytic antibacterial activity. However, there was

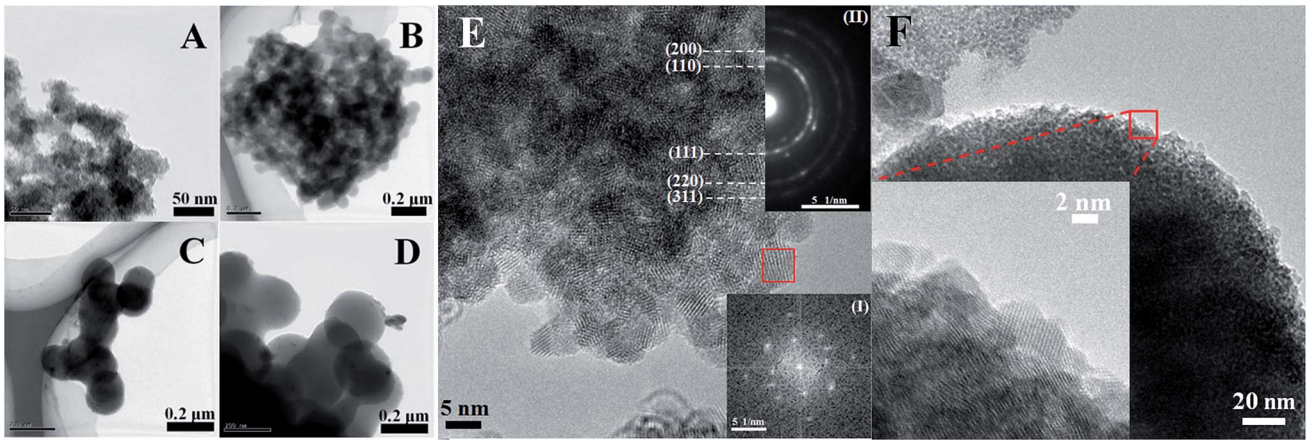

Fig. 3 TEM images of (A) Cu_2O-10, (B) Cu_2O-50, (C) Cu_2O-100 and (D) Cu_2O-200, and HRTEM images of (E) Cu_2O-10 and (F) Cu_2O-200. Insets (I) and (II) are the Fourier transform pattern corresponding to the red square region and the selected-area electron diffraction pattern corresponding to the whole of image E, respectively.

no significant difference in antibacterial activity between the VL irradiation and dark conditions for both low (5 μg mL^{-1}) and high (200 μg mL^{-1}) concentrations of Cu_2O-10. These results suggest that the inactivation of *E. coli* is dominated by its own antibacterial activity and its photocatalytic antibacterial activity is negligibly small when a low or high concentration of Cu_2O-10 is used. The inactivation kinetics of Cu_2O-10 with different concentrations under VL can all be fitted into the convex curves of the Weibull model (Table S2†). The very slight variation of the parameters p and δ (see and compare the rows highlighted with red in Tables S1(a) and S2†) further suggests that the antibacterial activity of Cu_2O was dominated by the toxicity of Cu_2O.

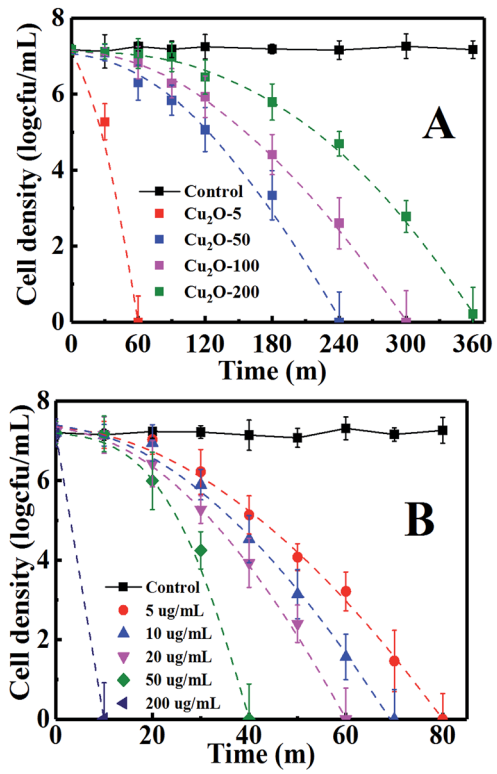

Fig. 4 Inactivation of *E. coli* by (A) 20 μg mL^{-1} of Cu_2O-10, Cu_2O-50, Cu_2O-100 and Cu_2O-200, respectively, in the dark and by (B) different amounts of Cu_2O-10. The log inactivation was plotted *versus* the time with dashed lines.

3.5. Mechanisms of inactivation of *E. coli* by Cu_2O NPs

3.5.1 Mechanisms of inactivation of *E. coli* by Cu_2O NPs in the dark. The origin of the antibacterial activities of Cu_2O in the dark was first investigated by Sunada *et al.*[34] who proposed that contact with the surface of Cu_2O caused denaturation or degradation of bacteria, resulting in their inactivation. This so-called "contact killing" was widely adopted by many researchers as a mechanism for the antibacterial activities of Cu_2O.[22,34,44] Meghana *et al.*[45] further proved that the cell envelope of bacteria initially suffered severe damage from Cu_2O, which added strong support to the contact killing mechanism. Here, we agree with the contact killing mechanism according to the results of the

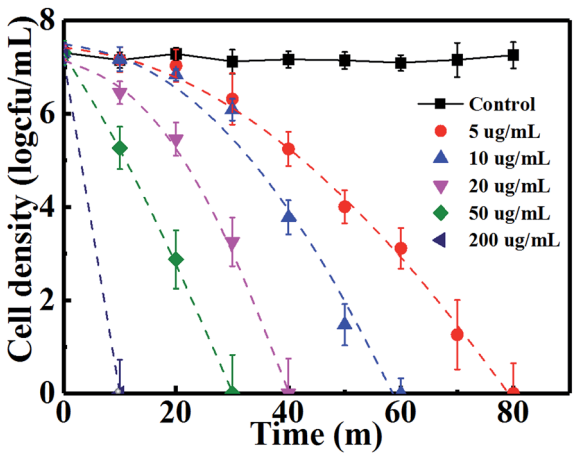

Fig. 5 Inactivation of *E. coli* by different amounts of Cu_2O-10 under VL.

antibacterial testing of Cu_2O-10 under aerobic and anaerobic conditions. As we know, reactive oxygen species (ROS) can be generated under aerobic conditions, but cannot exist in anaerobic conditions. Fig. S5† shows that Cu_2O-10 displayed the same inactivation efficiency in aerobic conditions (pink line) as in anaerobic conditions (blue line), suggesting that *E. coli* was inactivated by contact killing due to exclusion of the effect of ROS on the inactivation of the bacteria. In this case, the more contact between the Cu_2O-10 and bacterial cells, the higher the antibacterial activity was. Thus, it is expected that Cu_2O NPs with larger BET surface areas contribute a higher antibacterial activity. We determined the BET surface areas of Cu_2O-10, Cu_2O-50, Cu_2O-100 and Cu_2O-200 to be 26.24, 6.467, 4.421 and 3.228 $m^2\ g^{-1}$, respectively, which can demonstrate well that decreasing the size of the Cu_2O NPs results in increasing antibacterial activity. Similar size-dependent antibacterial activity was reported by B. Ajitha *et al.* who observed that the smallest size of Ag NPs displayed the highest antibacterial activity.[46]

3.5.2 Mechanisms of the inactivation of *E. coli* by Cu_2O NPs under VL. Under VL, Cu_2O acts as a photocatalyst. Photocatalysis is known to produce several ROS ($^{\bullet}OH$, H_2O_2, $^{\bullet}O_2^-$, and h^+) that are potentially involved in the inactivation of bacterial cells.[47] The roles of ROS for the photocatalytic inactivation of *E. coli* by Cu_2O-10 are clarified according to the scavenging study and testing results for ROS shown in Fig. 6. Scavengers are widely used to determine the bactericidal contribution of each reactive species, including sodium oxalate for h^+, isopropanol for $^{\bullet}OH$, TEMPOL for $^{\bullet}O_2^-$ and Fe(II)–EDTA for H_2O_2.[48–50] Before conducting the experiments, the applied concentration of each scavenger was optimized to ensure its maximum scavenging effect without causing any inactivation to the bacterial cell.[48–50] As discussed above, 20 μg mL^{-1} of Cu_2O-10 can inactivate 7-log of *E. coli* within 40 min. In this case, no scavenger was involved. With the addition of Fe(II)–EDTA (H_2O_2 scavenger) or isopropanol ($^{\bullet}OH$ scavenger), the inactivation of *E. coli* was partly prohibited, suggesting that both H_2O_2 and $^{\bullet}OH$ are primary ROS associated with the bacterial inactivation process. H_2O_2 and $^{\bullet}OH$ are generated through either an oxidative process or a reductive process. In an oxidative process, a hole can abstract electron from water and/or hydroxyl ions to produce $^{\bullet}OH$ and H_2O_2 (eqn (8) and (9)).

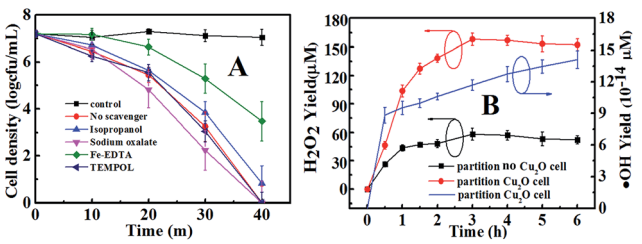

Fig. 6 (A) Photocatalytic inactivation of *E. coli* by Cu_2O-10 under VL irradiation with different scavengers (50 mmol L^{-1} sodium oxalate, 0.5 mmol L^{-1} isopropanol, 0.1 mmol L^{-1} Fe(II)–EDTA, and 2 mmol L^{-1} TEMPOL), and (B) H_2O_2 and $^{\bullet}OH$ yields in a partition system. The concentration of Cu_2O-10 was 20 μg mL^{-1}.

$$h^+ + H_2O \rightarrow {}^{\bullet}OH + H^+ \quad (8)$$

$$^{\bullet}OH + {}^{\bullet}OH \rightarrow H_2O_2 \quad (9)$$

However, the hole from the valence band of Cu_2O is produced at about +0.6 V potential, and no overpotential is available for the oxidation of water (about +0.57 V, eqn (9)).[28,51] It also cannot oxidize H_2O and OH^- to form H_2O_2 (+1.763 V) and $^{\bullet}OH$ (about +2.8 V), respectively. Thus, the origin of H_2O_2 and $^{\bullet}OH$ should be the electron from the conduction band of Cu_2O by a possible reductive process (eqn (10)–(13)).[29]

$$O_2 + e^- \rightarrow {}^{\bullet}O_2^- \quad (10)$$

$$O_2 + 2H_2O + 2e^- \rightarrow H_2O_2 + 2OH^- \quad (11)$$

$$^{\bullet}O_2^- + H_2O_2 \rightarrow {}^{\bullet}OH + OH^- + O_2 \quad (12)$$

$$H_2O_2 + e^- \rightarrow {}^{\bullet}OH + OH^- \quad (13)$$

It was observed that the addition of TEMPOL ($^{\bullet}O_2^-$ scavenger) did not significantly prohibit the inactivation of *E. coli*, suggesting that $^{\bullet}O_2^-$ was not involved in the bacterial inactivation. From Fig. S6,† one can see that no $^{\bullet}O_2^-$ signal was detected due to the absence of an absorption peak (470 nm), further confirming that $^{\bullet}O_2^-$ was not produced in the current conditions. In this case, the electrons followed the reductive process of eqn (11) and (13), through which H_2O_2 and $^{\bullet}OH$ were generated.

As mentioned above, h^+ is not involved in an oxidative process for the evolution of ROS. However, whether h^+ can directly inactivate *E. coli* or not needs to be clarified. Thus, sodium oxalate was used as a scavenger to determine the bactericidal contribution of h^+. Interestingly, the inactivation process was enhanced a bit (Fig. 6A) with the addition of sodium oxalate. This can be explained by the removal of h^+ by sodium oxalate enhancing the h^+–e^- separation efficiency, thus kinetically favoring the remaining e^- to form more ROS to inactivate cells in the system.[52] To eliminate the influence of e^- from the conduction band of Cu_2O, argon (Ar) was aerated to remove the dissolved O_2 in solution and hence prohibit the formation of ROS, leaving only the function of h^+ from the valence band. Control experiments with Ar in the dark and under VL (black and red curves in Fig. S5†) confirm that *E. coli* was not inactivated. In this case, the addition of sodium oxalate gave rise to the decrease in the inactivation efficiency (cyan and purple curves in Fig. S5†). This result indicates that when removing only the h^+ inactivation is inhibited, proving that h^+ on its own can directly inactivate the bacterial cells. Moreover, comparing the blue and green curves in Fig. S5,† one can conclude that the h^+ can directly kill the bacterial cells since Cu_2O-10 can more significantly inactivate *E. coli* under anaerobic conditions (green curve) than aerobic conditions (blue curve). Concerning holes produced at about +0.6 V, the holes can directly inactivate *E. coli* by electrochemically oxidizing coenzyme A (CoA) in the cell wall to dimeric CoA, resulting in the death of *E. coli*.[53]

3.6. The role of H_2O_2

The leading bactericidal effect of H_2O_2 rather than $^{\bullet}OH$ was expected because H_2O_2 production is thermodynamically favored by directly reducing O_2 to H_2O_2 (eqn (11)) while $^{\bullet}OH$ is produced through a second-order reaction (eqn (13)). This can be partly supported by the scavenging study data in Fig. 6. The addition of isopropanol inhibited the bacterial inactivation efficiency (over 6-log reduction) a little while the corresponding efficiency was greatly inhibited (only 1-log reduction) upon the addition of Fe(II)–EDTA, indicating that H_2O_2 is much more deeply involved in the disinfection than $^{\bullet}OH$. To explore the role of H_2O_2, we conducted a photocatalytic inactivation of *E. coli* using a partition system (Fig. S2†) and quantitatively assessed the H_2O_2 yield. The partition system was used to block direct contact between the bacterial cell and the Cu_2O, and excluded the function of toxicity of the Cu_2O, $^{\bullet}OH$ and h^+. Only H_2O_2 can diffuse across the membrane due to the long life of H_2O_2,[31] which is convenient for independent investigations on the inactivation of *E. coli* by H_2O_2. Fig. 6B shows that the H_2O_2 yields in both cells of the partition system increased at first and became stable over a prolonged time, due to the decomposition of H_2O_2 in parallel with its production.[54] The equilibrium concentrations of H_2O_2 in the Cu_2O cell and no-Cu_2O cell of the partition system were estimated to be 150 and 50 μM, respectively, which are much higher than the corresponding data (7.28 and 2.56 μM) from our previous Cu_2O film partition system.[31] The results indicate that Cu_2O-10 is a photocatalyst capable of highly-efficient H_2O_2 evolution. This ability of Cu_2O-10 for highly efficient H_2O_2 evolution is probably due to its high BET surface area and crystal structure with a high oriented (111) plane exhibiting higher photocatalytic activity than the other faces.[55,56] We observed that the 5-log *E. coli* was completely inactivated in the no-Cu_2O cell of the partition system within 7 h (Fig. 7). The inactivation efficacy of H_2O_2 in the no-Cu_2O cell was also confirmed by the BacLight kit fluorescent microscopic method (Fig. S7†). To investigate the dependence of the concentration of H_2O_2 on the antibacterial effect, we recorded the data of the inactivation of *E. coli* by direct addition of different concentrations of H_2O_2 (50–800 μM). A direct addition of H_2O_2 (50 μM) did not have significant antibacterial effect (Fig. 7). Note that the total amount of H_2O_2 was much higher than the actual measured value of 50 μM as H_2O_2 was generated continuously and dynamically consumed *in situ* in the system. Thus, the actual amount of H_2O_2 available to interact with the bacterial cell was much higher than the amount detected.[46] We observed that the equilibrium concentration of H_2O_2 was as high as 50 μM in the no-Cu_2O cell contributing to a similar inactivation efficiency to H_2O_2 (800 μM) (not shown in Fig. 7) by direct addition. The inactivation kinetics (dashed lines of Fig. 7) of *E. coli* by H_2O_2 in different conditions can be fitted into the shoulder-linear-tail model (eqn (2)). The rate of inactivation (K_{max}) increased and the shoulder length (S_l) decreased when the applied H_2O_2 concentration increased (Table S3†). Notably, the K_{max} of inactivation by 800 μM H_2O_2 (7.46 h^{-1}) is comparable to that of 50 μM H_2O_2 (7.49 h^{-1}) under VL.

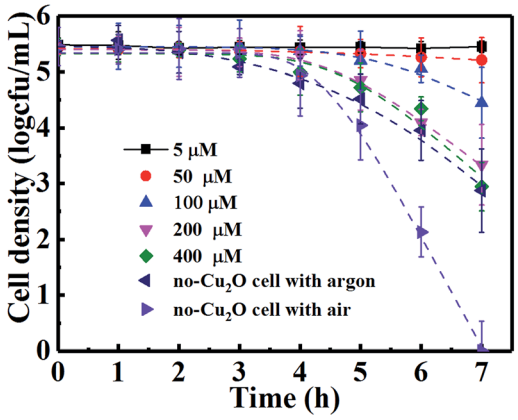

Fig. 7 Inactivation of *E. coli* by different amounts of H_2O_2 and in a no-Cu_2O cell of the partition system under VL irradiation.

3.7. The role of copper ions

Copper ion leakage from Cu_2O may contribute to the inactivation of *E. coli* because it is toxic at high concentrations[31,57] and underlying Fenton-like reactions (eqn (14) and (15)) produce ROS to inactivate *E. coli*.[57,58]

$$Cu(I) + O_2 \rightarrow Cu(II) + {}^{\bullet}O_2^- \quad (14)$$

$$Cu(I) + {}^{\bullet}O_2^- + 2H^+ \rightarrow Cu(II) + H_2O_2 \quad (15)$$

Fig. S8† shows the copper ion content, including the Cu^+ and Cu^{2+} leakage from a 20 μg mL^{-1} Cu_2O-10 suspension under irradiation and in the dark as a function of time. The copper ion leakage from Cu_2O-10 increased quickly in the first 2 h and slowly later, but with a low total leakage rate. After 7 h of VL irradiation, 0.34 mg L^{-1} of total copper ion (including 0.26 mg L^{-1} Cu^{2+} and 0.08 mg L^{-1} Cu^+) and 0.29 mg L^{-1} total copper ion (including 0.22 mg L^{-1} Cu^{2+} and 0.07 mg L^{-1} Cu^+) were present under VL and in the dark, respectively. The low concentration of copper ion leakage from Cu_2O-10 did not contribute to the antibacterial activity.[31] In addition, since $^{\bullet}O_2^-$ and $^{\bullet}OH$ were not detected, the copper-catalyzed Haber–Weiss reaction was probably too weak to be observed under the current experimental conditions. In all, the copper ion leakage from Cu_2O-10 did not contribute to the inactivation of *E. coli*.

4. Conclusions

In this study, a simplified and green approach for the size-controlled synthesis of Cu_2O nanoparticles (NPs) was achieved by chemical deposition technology. The obtained Cu_2O NPs presented size-dependent antibacterial activity, *i.e.* decreasing the size of the Cu_2O NPs resulted in increasing the antibacterial activity. The smallest size of Cu_2O-10 had a relatively low C of ≤1 μg mL^{-1} and enjoyed the highest antibacterial activity which could completely inactivate 7-log *E. coli* in 80 min with a concentration of 5 μg mL^{-1} in the dark. Under VL, the medium concentrations (10, 20 and 50 μg mL^{-1}) of Cu_2O-10 showed enhanced antibacterial activity compared with that in the dark, whereas low and high concentrations (5 and 200 μg

mL^{-1}) of Cu_2O-10 presented almost the same antibacterial activity as that in dark. "Contact killing" and ROS ($^{\cdot}OH$, H_2O_2 h^+) were found to be responsible for bacterial inactivation in the dark and under irradiation, respectively. Cu_2O-10 was proved to be effective for evolution of H_2O_2. A stable equilibrium concentration of H_2O_2 (as high as 150 μM) could be achieved by using 20 μg mL^{-1} Cu_2O-10 under VL. The inactivation kinetics of the Cu_2O NPs in different conditions and that of H_2O_2 were calculated and they were fitted into Weibull and shoulder-linear-tail models, respectively.

Conflicts of interest

There are no conflicts to declare.

Acknowledgements

This work was supported by the Natural Science Foundation of Hubei Province (2016CFB511), the Hubei Provincial Department of Education (D20152702), and the National Natural Science Foundation of China (11547018, 11647122, and 61705064). Dr Chen appreciates the support of the Project of the Open Fund of Hubei Key Laboratory of Ferro & Piezoelectric Materials and Devices (201605), the Outstanding Young and Middle-aged Innovation Team of Hubei (T201521) and the Major Project of Hubei Polytechnic University (16xjz03A).

References

1 A. S. Zoolfakar, R. A. Rani, A. J. Morfa, A. P. O'mullane and K. Kalantar-Zadeh, *J. Mater. Chem. C*, 2014, **2**, 5247.
2 W. Chen, W. Zhang, L. Chen, L. Zeng and M. Wei, *J. Alloys Compd.*, 2017, **723**, 172.
3 F. Wu, S. Banerjee, H. Li, Y. Myung and P. Banerjee, *Langmuir*, 2016, **32**, 4485.
4 M. Pang and H. C. Zeng, *Langmuir*, 2010, **26**, 5963.
5 D. Nunes, A. Pimentel, P. Barquinha, P. A. Carvalho, E. Fortunato and R. Martins, *J. Mater. Chem. C*, 2014, **2**, 6097.
6 K. X. Yao, X. M. Yin, T. H. Wang and H. C. Zeng, *J. Am. Chem. Soc.*, 2010, **132**, 6131.
7 A. Mishra and D. Pradhan, *Cryst. Growth Des.*, 2016, **16**, 3688.
8 M. Leng, M. Liu, Y. Zhang, Z. Wang, C. Yu, X. Yang, H. Zhang and C. Wang, *J. Am. Chem. Soc.*, 2010, **132**, 17084.
9 Q. Wang, Y. Jia, M. Wang, W. Qi, Y. Pang, X. Cui, W. Ji and J. Yi, *J. Phys. Chem. C*, 2015, **119**, 22066.
10 H. Xu, W. Wang and L. Zhou, *Cryst. Growth Des.*, 2008, **8**, 3486.
11 C. H. Kuo and M. H. Huang, *J. Am. Chem. Soc.*, 2008, **130**, 12815.
12 C. Tan, S. Hsu, W. Ke, L. Chen and H. Huang, *Nano Lett.*, 2015, **15**, 2155.
13 Y. Xu, H. Wang, Y. Yu, L. Tian, W. Zhao and B. Zhang, *J. Phys. Chem. C*, 2011, **115**, 15288.
14 W. Ke, C. Hsia, Y. Chen and H. Huang, *Small*, 2016, **12**, 3530.
15 L. Kiaune and N. Singhasemanon, *Rev. Environ. Contam. Toxicol.*, 2011, **213**, 1.
16 R. P. Allaker and K. Memarzadeh, *Int. J. Antimicrob. Agents*, 2014, **43**, 95.
17 W. Fan, X. Wang, M. Cui, D. Zhang, Y. Zhang, T. Yu and L. Guo, *Environ. Sci. Technol.*, 2012, **46**, 10255.
18 H. Pang, F. Gao and Q. Lu, *Chem. Commun.*, 2009, 1076.
19 J. Ren, W. Wang, S. Sun, L. Zhang, L. Wang and J. Chang, *Ind. Eng. Chem. Res.*, 2011, **50**, 10366.
20 K. Giannousi, G. Sarafidis, S. Mourdikoudis, A. Pantazaki and C. Dendrinou-Samara, *Inorg. Chem.*, 2014, **53**, 9657.
21 M. A. Vargas-Reus, K. Memarzadeh, J. Huang, G. G. Ren and R. P. Allaker, *Int. J. Antimicrob. Agents*, 2012, **40**, 135.
22 M. Hans, A. Erbe, S. Mathews, Y. Chen, M. Solioz and F. Mucklich, *Langmuir*, 2013, **29**, 16160.
23 J. Hrenovic, J. Milenkovic, N. Daneu, R. M. Kepcija and N. Rajic, *Chemosphere*, 2012, **88**, 1103.
24 C. H. Kuo, Y. C. Yang, S. Gwo and M. H. Huang, *J. Am. Chem. Soc.*, 2011, **133**, 1052.
25 A. Singhal, M. R. Pai, R. Rao, K. T. Pillai, I. Lieberwirth and A. K. Tyagi, *Eur. J. Inorg. Chem.*, 2013, **2013**, 2640.
26 S. Kakuta and T. Abe, *Electrochem. Solid-State Lett.*, 2009, **12**, P1.
27 M. K. I. Senevirathna, P. K. D. D. P. Pitigala and K. Tennakone, *J. Photochem. Photobiol., A*, 2005, **171**, 257.
28 P. E. De Jongh, D. Vanmaekelbergh and J. J. Kelly, *J. Electrochem. Soc.*, 2000, **147**, 486.
29 L. Xiong, H. Yu, G. Yang, M. Qiu, J. Chen and Y. Yu, *Thin Solid Films*, 2010, **518**, 6738.
30 L. Huang, F. Peng, H. Yu and H. Wang, *Solid State Sci.*, 2009, **11**, 129.
31 L. Xiong, T. W. Ng, Y. Yu, D. Xia, H. Y. Yip, G. Li, T. An, H. Zhao and P. K. Wong, *Electrochim. Acta*, 2015, **153**, 583.
32 Y. Zhang, L. Ma, J. Li and Y. Yu, *Environ. Sci. Technol.*, 2007, **41**, 6264.
33 A. H. Geeraerd, C. H. Herremans and J. F. Van Impe, *Int. J. Food Microbiol.*, 2000, **59**, 185.
34 K. Sunada, M. Minoshima and K. Hashimoto, *J. Hazard. Mater.*, 2012, **235–236**, 265.
35 M. W. Sutherland and B. A. Learmonth, *Free Radical Res.*, 1997, **27**, 283.
36 Y. Li, W. Zhang, J. Niu and Y. Chen, *ACS Nano*, 2012, **6**, 5164.
37 L. Brunet, D. Y. Lyon, E. M. Hotze, P. J. J. Alvarez and M. R. Wiesner, *Environ. Sci. Technol.*, 2009, **43**, 4355.
38 K. Ishibashi, A. Fujishima, T. Watanabe and K. Hashimoto, *J. Photochem. Photobiol., A*, 2000, **134**, 139.
39 H. Xu, W. J. Cooper, J. Jung and W. Song, *Water Res.*, 2011, **45**, 632.
40 D. Zhang, S. Yan and W. Song, *Environ. Sci. Technol.*, 2014, **48**, 12645.
41 M. a. J. S. Van Boekel, *Int. J. Food Microbiol.*, 2002, **74**, 139.
42 M. Peleg and M. B. Cole, *Crit. Rev. Food Sci. Nutr.*, 1998, **38**, 353.
43 M. Turalija, P. Merschak, B. Redl, U. Griesser, H. Duelli and T. Bechtold, *J. Mater. Chem. B*, 2015, **3**, 5886.
44 G. S. Theja, R. C. Lowrence, V. Ravi, S. Nagarajan and S. P. Anthony, *CrystEngComm*, 2014, **16**, 9866.
45 S. Meghana, P. Kabra, S. Chakraborty and N. Padmavathy, *RSC Adv.*, 2015, **5**, 12293.

46 B. Ajitha, Y. Reddy, P. Reddy, H. Jeon and C. Ahn, *RSC Adv.*, 2016, **6**, 36171.
47 W. Wang, L. Zhang, T. An, G. Li, H. Yip and P. Wong, *Appl. Catal., B*, 2011, **108–109**, 108.
48 Y. Chen, A. Lu, Y. Li, L. Zhang, H. Y. Yip, H. Zhao, T. An and P. K. Wong, *Environ. Sci. Technol.*, 2011, **45**, 5689.
49 W. Wang, Y. Yu, T. An, G. Li, H. Y. Yip, J. C. Yu and P. K. Wong, *Environ. Sci. Technol.*, 2012, **46**, 4599.
50 L. S. Zhang, K. H. Wong, D. Q. Zhang, C. Hu, J. C. Yu, C. Y. Chan and P. K. Wong, *Environ. Sci. Technol.*, 2009, **43**, 7883.
51 P. E. De Jongh, D. Vanmaekelbergh and J. J. Kelly, *Chem. Commun.*, 1999, 1069.
52 D. Xia, Z. Shen, G. Huang, W. Wang, J. C. Yu and P. K. Wong, *Environ. Sci. Technol.*, 2015, **49**, 6264.
53 T. Matsunaga, Y. Namba and T. Nakajima, *Bioelectrochem. Bioenerg.*, 1984, **13**, 393.
54 F. Shiraishi and C. Kawanishi, *J. Phys. Chem. A*, 2004, **108**, 10491.
55 L. Feng, C. Zhang, G. Gao and D. Cui, *Nanoscale Res. Lett.*, 2012, **7**, 1.
56 H. Xu, W. Wang and W. Zhu, *J. Phys. Chem. B*, 2006, **110**, 13829.
57 H. J. Park, T. T. Nguyen, J. Yoon and C. Lee, *Environ. Sci. Technol.*, 2012, **46**, 11299.
58 N. Perez-Almeida, M. Gonzalez-Davila, J. M. Santana-Casiano, A. G. Gonzalez and M. Suarez De Tangil, *Environ. Sci. Technol.*, 2013, **47**, 1239.